

## TSUNAMI MODELLING ON UNSTRUCTURED GRIDS: VERIFICATION AND VALIDATION

ALEXEY ANDROSOV<sup>1</sup>, SVEN HARIG<sup>1</sup>, JÖRN BEHRENS<sup>1</sup>, JENS SCHRÖTER<sup>1</sup>, AND  
SERGEY DANILOV<sup>1</sup>

<sup>1</sup> Alfred Wegener Institute for Polar and Marine Research, 27570 Bremerhaven, Germany  
(Alexey.Androssov@awi.de)

**ABSTRACT:** After the destructive event of December 26, 2004, many attempts have been made to accurately simulate the generation and propagation of tsunami waves in the Indian Ocean. In support of the Tsunami Early Warning System for the Indian Ocean, a very high-resolution finite element model (*TsunAWI*) has been developed for simulations of the wave propagation. It offers geometrical flexibility by working on unstructured triangular grids and is based on finite-element  $P_1^{NC} - P_1$  discretization. The paper offers a brief description of the model, with a focus on its verification and validation. The key issue in modelling the tsunami is wetting and drying. The original algorithm to solve this problem is discussed. Full and reduced formulation of the momentum advection for  $P_1^{NC} - P_1$  elements and parameterization of horizontal diffusion are presented. Using the well-known Okushiri test case, the influence of nonlinearity on the wave propagation is demonstrated. Numerical experiments simulating the Indian Ocean Tsunami on December 26, 2004 have been conducted. For the whole Indian Ocean, the comparison of simulation results with observational (coast gauge) data is carried out. The inundation obtained in simulations compares well to field measurements and satellite images of Banda Aceh region.

### 1. INTRODUCTION

In support of the Tsunami Early Warning System for the Indian Ocean, a finite element model *TsunAWI* for simulations of wave propagation has been developed. It is part of the German Indonesian Tsunami Early Warning System (GITEWS) serving to predict arrival times and expected wave heights. The finite-element (FE) spatial discretization allows for unstructured triangular meshes of variable resolution.

Finite-element methods are widely used in studies of wave generation and propagation in different fields of fluid dynamics. They are often employed to simulate propagation of long waves such as ocean tides and tsunamis in the ocean in the framework of shallow-water equations (Kienle *et al.*, 1987; Greenberg *et al.*, 1993; Baptista *et al.*, 1993). The main reason to prefer FE modelling is that the solution is computed over a grid that can be adapted to cover basins with complex geometries characterized by irregular bottom topography and coastlines. This is exactly what is needed in the framework of GITEWS.

Although several FE codes dealing successfully with wave propagation in complex geometries exist, the search for numerically efficient and accurate algorithms gives birth for new designs.

The main goal of this paper is twofold. First, we give a description of the shallow water model used by us. Following Hanert *et al.*, (2005), the model employs continuous linear representation ( $P_1$ ) for elevation and discontinuous, nonconforming, linear representation for the velocity ( $P_1^{NC}$ ). In contrast to Hanert *et al.* (2005), it uses a different time stepping scheme and offers three stable versions of momentum advection discretization versus the unstable one in the original approach. Second, we test the model performance against an analytical solution for a channel test case, an experimental test case (the Okushiri test) and observational data related to the tsunami event of December 26, 2004.

The paper is organized as follows. In Section 2, the spatial and temporal discretization of the model is presented. Section 3 deals with its verification and validation. Section 4 concludes the presentation.

## 2. BAROTROPIC SHALLOW WATER MODEL

### 2.1 Boundary-value problem in Cartesian coordinates

Consider vertically averaged equations of motion and continuity in  $\tilde{\Omega} = \{x, y \subset \Omega, 0 \leq t \leq T\}$ , where  $\Omega$  is a plane domain bounded by boundary  $\partial\Omega$ ,

$$\mathbf{v}_t + (\mathbf{v} \cdot \nabla)\mathbf{v} + g\nabla\zeta = \Phi \equiv f\mathbf{k} \times \mathbf{v} - rH^{-1}\mathbf{v}|\mathbf{v}| + H^{-1}\nabla(K_h H\nabla\mathbf{v}), \quad (1)$$

$$\zeta_t + \nabla \cdot (H\mathbf{v}) = 0. \quad (2)$$

Here  $\mathbf{v} = (u, v)$  is the velocity vector,  $H = h + \zeta$  the total water depth,  $H > 0$ ,  $h$  is the unperturbed water depth, and  $\zeta$  the surface elevation,  $\nabla = (\partial/\partial x, \partial/\partial y)$  is the gradient operator,  $f$  the Coriolis parameter,  $\mathbf{k}$  the unit vector in the vertical direction,  $r$  the bottom friction coefficient, and  $K_h$  the eddy viscosity coefficient. The set of (1) and (2) is known as the rotating shallow water equations. On the solid part of the boundary,  $\partial\Omega_1$ , and on its open part,  $\partial\Omega_2$ , we impose the following boundary conditions

$$v_n|_{\partial\Omega_1} = 0, \quad \Gamma(\mathbf{v}, \zeta)|_{\partial\Omega_2} = \Xi_1, \quad (3)$$

where  $v_n$  is the velocity normal to  $\partial\Omega_1$ ,  $\Gamma$  is the operator of the boundary conditions and  $\Xi_1$  is a vector-function determined by the boundary regime and different for inflow and outflow (Oliger and Sundström, 1978). In practice, when the full necessary information on the open boundary is unavailable, in place of the second condition (3) one commonly imposes the boundary condition on the elevation  $\zeta|_{\partial\Omega_2} = \psi(x, y, t)$  or the radiation boundary condition  $u_n = \mathbf{v} \cdot \mathbf{n} = \sqrt{\frac{g}{H}}\zeta$ . The latter provides free linear wave passage through the open boundary (when the Coriolis acceleration plays a small role). Here  $\mathbf{n}$  is the outer unit normal to  $\partial\Omega_2$ . The accuracy of the reduced boundary-value formulation with only the sea level assigned at the open boundary, was analyzed by Androsov et al (1995). The problem (1)-(3) for the combination  $\mathbf{u} = (\mathbf{v}, \zeta)$  is solved for given initial conditions:

$$\mathbf{u}|_{t=0} = \mathbf{u}^0. \quad (4)$$

### 2.2 The non-conforming mixed $P_1^{NC} - P_1$ discretization

#### 2.2.1 Spatial discretization

The finite element spatial discretization is based on the approach by Hanert et al. (2005) with some modifications like added viscous and bottom friction terms, corrected momentum advection terms, radiation boundary condition and nodal lumping of mass matrix in the continuity equation. The basic principles of discretization follow the paper of Hanert et al. (2005) and are not repeated here.

#### 2.2.2 Time discretization

Simulation of tsunami wave propagation benefits from using an explicit time discretization. Indeed, numerical accuracy requires relatively small time steps, which reduces the main advantage of implicit schemes. Furthermore, modelling the inundation processes usually requires very high spatial

resolution in costal regions (up to some tens of meters) and consequently large number of nodes, drastically increasing necessary computational resources in case of implicit temporal discretization.

The leap-frog discretization was chosen as a simple and easy to implement method. We rewrite Equations 1 and 2 in time discrete form,

$$\frac{\mathbf{v}^{n+1} - \mathbf{v}^{n-1}}{2\Delta t} + f\mathbf{k} \times \mathbf{v}^n + g\nabla \zeta^n + \frac{r}{H^n} |\mathbf{v}^n| \mathbf{v}^{n+1} - \nabla K_h \nabla \mathbf{v}^{n-1} + (\mathbf{v}^n \nabla) \mathbf{v}^n = 0, \quad (5)$$

$$\frac{\zeta^{n+1} - \zeta^{n-1}}{2\Delta t} + \nabla \cdot (H^n \mathbf{v}^n) = 0. \quad (6)$$

Here  $\Delta t$  is the time step length and  $n$  the time index. The leap-frog three-time-level scheme provides second-order accuracy and is neutral within the stability range. This scheme however has a numerical mode which is removed by the standard filtering procedure.

### 2.3 Momentum advection schemes

The experience with  $P_1^{NC} - P_1$  code reveals problems with spatial noise and instability of the momentum advection if the discretization is used in the form described by Hanert et al. (2005). Here we suggest a regular procedure to derive the FE discretization with discontinuous functions which guarantees consistency with the original governing equations. Applying this procedure shows that a term is missing from the discretization of momentum suggested in the paper cited above. It serves to penalize discontinuity of normal velocity across the edges.

#### 2.3.1 Consistent $P_1^{NC}$ discretization

We leave continuous test/basic functions as they are, but augment the discontinuous  $P_1^{NC}$  functions by defining them in the following way:

$$\Psi_{ie}(x, y) = \Theta_e \psi_{ie}(x, y). \quad (7)$$

In this definition,  $\Theta_e(x, y) = 1$ , if point  $(x, y)$  is inside element  $e$ , 0 if it is outside and  $1/2$  if it is on the boundary, and  $\psi_{ie}(x, y)$  is the  $P_1^{NC}$  basis function due to edge  $i$  on element  $e$ . The test/basis function  $\Psi$  are now defined everywhere so that we can work with them as in the continuous case.

We write

$$(\mathbf{u} \nabla) \mathbf{u} = (\mathbf{u} t \partial_t + \mathbf{u} n \partial_n) \mathbf{u} \quad (8)$$

based on tangential and normal directions associated with edge  $i$ . Only the second term contains a singularity at the edge and we will further continue with this singularity. In the vicinity of the edge it can be written as

$$[(\mathbf{u} \nabla) \mathbf{u}] = (\mathbf{u}_f + \Theta(y)(\mathbf{u}_e - \mathbf{u}_f)) \mathbf{h} \delta(y)(\mathbf{u}_e - \mathbf{u}_f) \quad (9)$$

Here the coordinates  $x$  and  $y$  are transformed, so that  $x$  is tangential and  $y$  is perpendicular to the edge  $i$ , subscript  $s$  implies that only the singular part is taken into account, and  $e$  and  $f$  denote elements sharing edge  $i$ , with the normal vector pointing to  $e$  by. This implies that the singular part of

$$\int \hat{\mathbf{u}} (\mathbf{u} \nabla) \mathbf{u} dS \quad (10)$$

due to edge  $i$  is the integral over a small vicinity of this edge

$$\int_i (\hat{\mathbf{u}}_f + \Theta(y)(\hat{\mathbf{u}}_e - \hat{\mathbf{u}}_f)) (\mathbf{u}_f + \Theta(y)(\mathbf{u}_e - \mathbf{u}_f)) \mathbf{h} \delta(y) (\mathbf{u}_e - \mathbf{u}_f) dS \quad (11)$$

Representing  $dS$  as  $dx dy$  and using the notation  $[\mathbf{u}] = \mathbf{u}_e - \mathbf{u}_f$  and  $\langle \mathbf{u} \rangle = \frac{1}{2}(\mathbf{u}_e + \mathbf{u}_f)$  one performs integration over  $y$  first to get the following result (and omitting terms that would vanish after integration over  $x$ ).

$$-\int_i \hat{\mathbf{u}}_f \langle \mathbf{u} \rangle [\mathbf{u}] dx + \frac{1}{2} \int_i [\hat{\mathbf{u}}]_f \mathbf{n} [\mathbf{u}] dx = -\int_i (\langle \hat{\mathbf{u}} \rangle \langle \mathbf{u} \rangle) - (1/4) [\hat{\mathbf{u}}] [\mathbf{u}] dx \quad (12)$$

The last term in this expression can be omitted as it will disappear on performing integration along the edge. The remaining term should be added on all edges to get a consistent discretization of the momentum advection. To see the difference to the approach by Hanert et al. (2005) we further integrate the elemental integrals by parts to finally get

$$\int \hat{\mathbf{u}} (\mathbf{u} \nabla) \mathbf{u} dS = - \sum_{ed} \int_{ed} \mathbf{u} \nabla (\hat{\mathbf{u}} \cdot \mathbf{u}) dS + \sum_{ed} \int_{ed} (\langle \hat{\mathbf{u}} \rangle \langle \mathbf{u} \rangle [\mathbf{u} \mathbf{n}] + [\hat{\mathbf{u}}] \langle \mathbf{u} \rangle \langle \mathbf{u} \mathbf{n} \rangle + (1/2) [\hat{\mathbf{u}}] [\mathbf{u}] [\mathbf{u} \mathbf{n}]) d\Gamma. \quad (13)$$

The last term in the integral over edges will disappear after integration and thus can be removed from this expression. If we compare the remaining form with that given in Hanert et al. (2005) (without upwinding) it can be readily noticed that the term penalizing jump of normal velocity  $[\mathbf{u} \mathbf{n}]$  is absent there. Upwind terms can be added separately.

### 2.3.2 $P_1$ projection method

The consistent implementation of the momentum advection involves cycling over edges in the numerical code, in addition to cycling over elements to assemble the elemental contributions. This is not very convenient. In addition, it was found that while consistent implementation works well, it still requires some viscous dissipation for removing small-scale noise in the velocity field. This lead us to a simpler approach, which provides some smoothing of the velocity fields while removing edge contributions.

According to these approaches, to calculate the advection term in the momentum equation we first project the velocity from the  $P_1^{NC}$  to the  $P_1$  space in order to smooth it. To make this projection numerically effective, nodal quadrature (lumped mass matrix) is used. Then we use the projected velocity to estimate the advection term and proceed as usual by multiplying the result with a  $P_1^{NC}$  basis functions and integrating over the domain. This results in a very stable behaviour. In case of the combined discretization  $P_1^{NC} - P_1$  of advective transport, only velocity subject to differential operation is taken from space  $P_1$ . The consistent non-conforming velocity is used as advecting one. This approach should formally be more accurate. Since in these cases one differentiates the continuous velocity, no singular contributions appear. Thus in contrast to the consistent  $P_1^{NC}$  advection scheme both approaches do not lead to boundary integrals. To distinguish these approaches from the full non-conforming implementation we will call them  $P_1$  advection and  $P_1^{NC} - P_1$  advection, respectively.

### 2.4 Other implementation details (wetting and drying, viscosity)

Wave run-up generated by a tsunami reaching the shoreline may induce devastating flood waves. A tsunami is a long-period wave generated by ocean bottom motion during an earthquake with wave

length of about 200 to 350 km. Although the wave amplitude is moderate in deep waters, the tsunami wave slows down and the wave height increases near the shoreline until it breaks. The wave run-up height might reach several metres above the natural sea level and cause significant damage. Seamless simulation of wetting and drying is needed even in far field forecasting, at least to avoid artificial wave reflections from the coast which occur if a “solid boundary” is assumed there.

In our study we adjust the continuity and momentum balance equations in the way that they provide a reasonable solution in the dry regions, i.e. zero velocities and surface elevation equal to land topography. The computational domain is extended over the land. The continuity equation is adjusted by replacing the total depth  $H$  with  $H_+ = \max(H, 0)$ . In the momentum equation, full  $H$  enters only the bottom friction term. Here we use a standard approach bounding the total depth with some critical value  $H_{cr}$ , i.e.  $H$  in the friction term denominator is replaced with  $\max(H, H_{cr})$ . The next term one takes care about is the sea surface gradient. A special treatment is required for so-called “semi-dry” elements, i.e. elements with one or two dry and, correspondingly two or one wet vertices. For modelling wetting and drying we use a moving boundary technique which utilizes linear least square extrapolation through the wet-dry boundary and into the dry region. We apply “dry node concept” developed by Lynett 2002. The idea of this concept is to exclude dry nodes from the solution and then to extrapolate elevation to the dry nodes from their wet neighbours. The number of “wet” points in this case should be not less than 4. The aim of this method is to find a plane (representing the elevation or gradient), given by the linear parametric representation

$$f(x, y) = a_0 + a_1x + a_2y \quad (14)$$

with  $(a_0, a_1, a_2)$  a parameter triplet. With the least squares approach,  $f$  can be found by requiring it to be the best fit with respect to the  $L_2$ -norm:

$$\|f(x, y) - a_0 - a_1x - a_2y\|_2 = \min \quad (15)$$

Because the scheme is neutrally stable it demands horizontal viscosity in places of the large gradients of the solution. Although the initial perturbation is as a rule smooth, large gradients may form due to nonlinear steepening of the wave front or on reflections from jumps in topography or coast. Using uniform horizontal viscosity on non-uniform grids is a very poor choice leading to strong limitation on time stepping. Using the coefficient depending on the grid size proved to be not efficient too as one needs high viscosity only when large velocity gradients are observed. For this reason the coefficient of horizontal viscosity was determined according to the Smagorinsky parameterization

$$K_h = c \, dxdy \sqrt{\left(\frac{\partial u}{\partial x}\right)^2 + \frac{1}{2}\left(\frac{\partial v}{\partial x} + \frac{\partial u}{\partial y}\right)^2 + \left(\frac{\partial v}{\partial y}\right)^2} \quad (16)$$

The product of mesh cell sizes  $dxdy$  is replaced by areas of elements in the code while the adjustable coefficient  $c$  is set to 0.04 – 0.4. These are about the smallest values that can be used while maintaining numerical stability.

We take advantage of the explicit approach and accelerate the model at the beginning of tsunami wave propagation. If one has a local source like an earthquake there is no need to integrate model equations over the whole computational domain especially if the model covers whole the ocean. To avoid unnecessary computations we split the domain in 1 per 1 degree squares and collect the element numbers lying in every square. The integration is carried out only within rectangles with non-zero sea surface elevation. This simple trick implemented to the Indian Ocean tsunami model based on approx. 2 million nodes accelerated the computational time up to 20 times for the first hour of the wave propagation.

### 3. RESULTS

#### 3.1 Momentum advection tests

To test the impact of the momentum advection discretization on wave propagation, a test case simulation has been performed. It deals with a wave in the narrow channel with solid boundaries and underwater sill (see Fig. 1a). The initial conditions for elevation (10 m of amplitude) and horizontal velocity specify a wave propagating along the channel. The grid contains approximately 150000 nodes (the number of elements is twice as large). When propagating over a flat part of the bottom the wave form practically preserves for all types of advection as nonlinearity plays a very limited role there. Yet on passing over the hill the amplitude of wave increases drastically and nonlinear effects become significant.

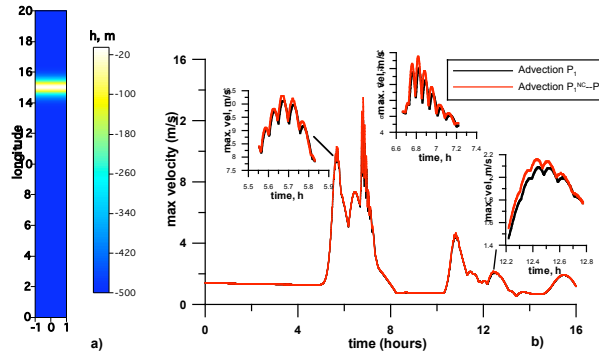


Fig. 1. a) Computational domain with bathymetry. b) Comparison maximal velocity for two representation of advection: correct  $P_1^{NC}$  (red lines) and reduced  $P_1$  (black lines).

Figure 1b compares the maximum velocity as a function of time for two variants of the momentum advection term. As it is apparent from Fig. 1b, there is a very good agreement between the two cases, with  $P_1^{NC} - P_1$  advection providing slightly higher amplitudes as expected. The simulation with consistent non-conforming momentum advection showed very similar behaviour too, but required higher values of viscosity for numerical stability. We conclude that all forms of momentum advection can be safely used, but the two with re-projection require less care in tuning friction and viscosity, and less computational effort. They are a preferred choice.

#### 3.2 Wetting and drying.

The classic analytical solution for wave run-up on a sloping beach was first expressed by Carrier and Greenspan (1958) and later revisited by Siden and Lynch (1988). To test the performance of our wetting and drying algorithm we simulate wave perturbation onshore for the case of linearly varying depth which admits of this analytical solution.

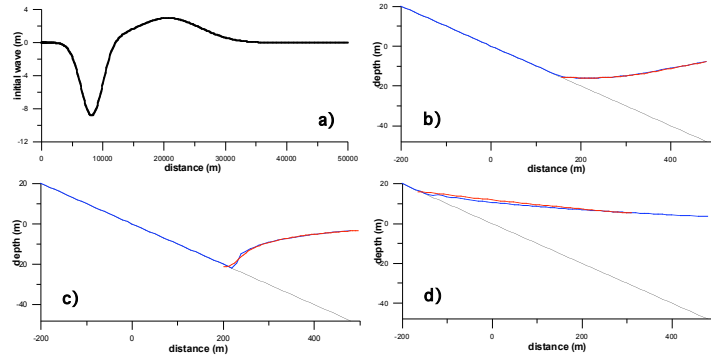


Fig. 2. Tsunami run-up on a plane beach. a) initial wave; b) run-up after 160 sec; c) run-up after 175 sec.; run-up after 220 sec. Red and blue curves correspond to analytical and numerical solutions, respectively.

Figure 2 compares the wave form simulated with the numerical model (with nonlinear terms switched off) against the analytical solution for several moments of time. Apparently, the numerical solution is in the good agreement with the analytical result. Some difference is observed in the vicinity of front and can be explained by several factors among which presence of horizontal diffusion (which is absent in the analytical solution) is most likely one.

### 3.3 The Okushiri test case

The 1993 Okushiri tsunami caused many unexpected phenomena. One of them was the extreme run-up height of 32 m that was measured near the village of Monai in Okushiri Island. This benchmark problem is a simulation of a 1/400 scale laboratory experiment of the Monai run-up, performed in a large-scale tank (205 m long, 6 m deep, 3.4 m wide) at Central Research Institute for Electric Power Industry (CRIEPI) in Abiko, Japan.

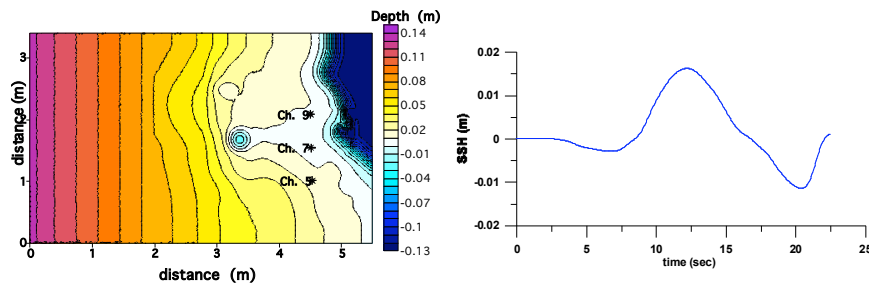


Fig. 3. a) Computational / experimental domain with bathymetry. Stars mark wave gage positions; b) Input wave.

The bathymetry and coastal topography used in the laboratory experiment are shown in Fig. 3. Three stations marked by stars in the figure provided the elevation used for the comparison. We note that right, top and bottom boundaries (in the figure plane) are solid and the left boundary is open. The numerical mesh covers the area of the experiment. The initial tsunami wave is imposed at the open boundary and shown in Fig. 3b. Its duration is 22.5 s.

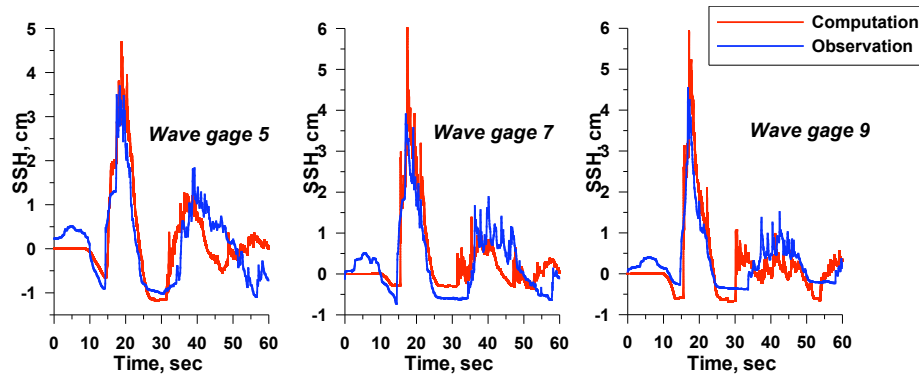


Fig. 4. Comparison experimental data (blue lines) with numerical simulation (red lines) for the Okushiri test case in runs without momentum advection.

To illustrate the importance of the momentum advection in getting agreement with observations simulations of the Okushiri test were performed in runs without (Fig. 4) and with the momentum advection (Fig. 5). It is noteworthy that the first maximum in Fig. 4 agrees well with respect to phase and is slightly overestimated with respect to amplitude. The second maximum leads the observational data for approximately 5 seconds, yet shows reasonable amplitude.

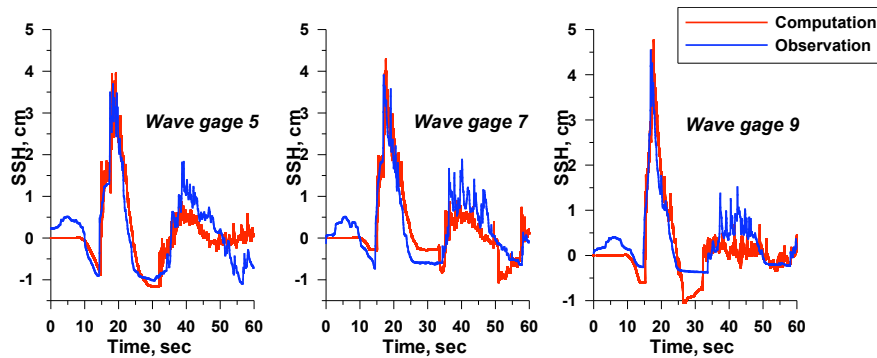


Fig. 5. Comparison experimental data (blue lines) with numerical simulation (red lines) for the Okushiri test case in runs with the momentum advection.

Including the momentum advection noticeably improves the agreement. In this case, both the first and second maxima are reproducing the observations very well as regards their phase. The amplitude of the first maximum shows almost perfect agreement with observations. It is necessary to note that the laboratory data contain some spurious elevation during the early phase of the experiment (which does not agree with the initial wave shape).

This test case is rather sensitive to the magnitude of viscosity and bottom drag used in numerical simulations and indeed requires the Smagorinsky viscosity to get the agreement in amplitudes.

### 3.4 Tsunami simulation

For the purpose of model verification in realistic situations over long time scales we simulate tsunami wave propagation in the entire Indian Ocean. For this purpose, the mesh for the Indian Ocean was designed. It consist of 2166320 nodes (4304458 elements) and has min distance of 500 m. The event

is the devastating tsunami of 26 December 2004. The observed elevation at several tide gauges across the Indian Ocean is used for the comparison shown in Fig. 6.

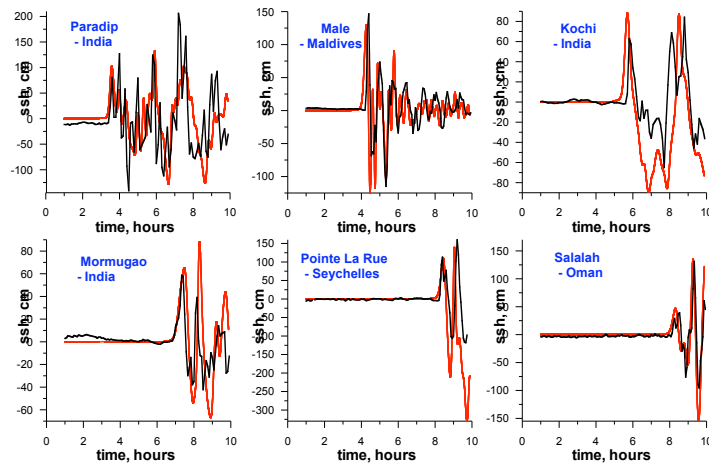


Fig. 6 Numerical experiments simulating the Indian Ocean Tsunami generated by the earthquake of December 26, 2004. Comparison of the computed elevation (red line) with the observed one (black line) at different location.

Given still only approximately known parameters of the tsunami source the coincidence between the model and observation is indeed good. Not only the arrival time of the first wave is reliably simulated, but the entire shape of the signal is reproduced reasonably well, and with correct amplitude. This proves the skill of the model as a tool to simulate tsunami wave propagation.

#### 4. CONCLUSION

The combination of non-conforming velocity with linear elevation suggests a well-rounded choice for shallow-water modelling on unstructured triangular grids, with a particular focus on simulating tsunami wave propagation. Although our approach was initially inspired by the algorithm proposed by Hanert et al. (2005) the resulting model is essentially different from it in a number of key directions. First, it is equipped with wetting and drying algorithms and can simulate inundation caused by tsunami. Second, it suggests a choice of stably working discretizations of the momentum advection which all improve over the original method of Hanert et al. (2005) and differ between themselves in a degree of smoothing applied. Third, it uses the Smagorinsky horizontal viscosity which is crucial for keeping the dissipation on the level that does not affect the quality of the solution. Finally, the explicit time stepping made possible through the nodal quadrature of the time derivative term in the continuity equation ensures numerically efficient performance while providing a straightforward and easy to implement algorithm.

The performance of the model is tested against observational data (the Okushiri test case and the Indian Ocean Tsunami of December 26, 2004) and the analytical solution by Carrier et al. (2003) and proves to be reasonably good showing the high level of realism sufficient for predicting the propagation of tsunami waves.

The model can be considered as an easy to use and reliable tool which not only serves the purposes of GITEWS but can be employed for other tasks which can be described in the framework of shallow water equations (with exception of true shock waves for which continuous elevation is a suboptimal choice).

## 5. REFERENCES

- Androsov, A.A., Klevanny K.A., Salusti E.S. and Voltzinger N.E. (1995). "Open boundary conditions for horizontal 2-D curvilinear-grid long-wave dynamics of a strait", *Adv. Water Resour.*, Vol. 18, 267-276.
- Baptista, A. M., Priest, G. R. and Murty, T. S. (1993). "Field survey of the 1992 Nicaragua Tsunami", *Marine Geodesy*, Vol. 16, 1692-1703.
- G.F. Carrier, G.F., Greenspan, H.P. (1958) "Water waves of finite amplitude on a sloping beach", *Journal of Fluid Mechanics*, Vol. 4, 97-109.
- Greenberg, D. A., Murty, T. S. and Ruffman, A. (1993). "A numerical model for the Halifax Harbor tsunami due to the 1917 explosion", *Marine Geodesy*, Vol. 16, 153-167.
- Kienle, J., Kowalik, Z. and Murty, T. S. (1987), "Tsunamis generated by eruptions from Mount St. Augustine Volcano, Alaska", *Science*, Vol. 236, 1442-1447.
- Lynett, P.J., Wu, T.-R., Liu, P.L.-F. (2002), "Modeling wave runup with depth-integrated equations", *Coastal Engineering*, Vol. 46, 89– 107.
- Hanert, E., Le Roux, D. Y., Legat V. and Delesnijder, E. (2005). "An efficient Eulerian finite element method for the shallow water equations", *Ocean Modelling*, Vol. 10, 115-136.
- Olinger, J. and Sundström A. (1978). "Theoretical and practical aspects of some initial boundary value problems in fluid dynamics", *SIAM J Appl Math.*, Vol. 35, 419-446.
- Siden, G.L.D Lynch, D.R. (1988) "Wave Equation Hydrodynamics on Deforming Elements", *International Journal for Numerical Methods in Fluids*, Vol. 8, 1071-1093.